Project Report 21158: Beyond the damage zone: Characterizing widespread inelastic deformation from surficial fractures and aftershocks of the Ridgecrest sequence

Summary

We use post-earthquake lidar data to remotely map surface ruptures produced by the 2019 Ridgecrest Earthquake sequence. The 4 July Mw 6.4 and 5 July Mw 7.1 earthquakes produced surface rupture zones approximately 20 km and 50 km in length, respectively. Intensively ruptured zones span up to four kilometers in width for both events, with numerous surficial fractures occurring more than 10 km from the main rupture. The purpose of this study is to develop an objective, uniform map product from which we test 1) the reproducibility of remote surface-rupture mapping between individual remote mappers and 2) the accuracy of remote compared to field-derived surface-rupture mapping. A second purpose of this study is to quantitatively analyze the overall distribution of surface ruptures for this event. The first phase of this project was remote mapping of the surface rupture by three independent mappers with various backgrounds in active tectonics. This mapping was done from the post-earthquake airborne lidar (Hudnut et al., 2020), without input from post-earthquake field mapping. Visual comparison of the three remote rupture maps show good agreement for scarps accommodating vertical displacements exceeding 50 cm. For features with smaller vertical displacements, interpretations of the data vary more widely between mappers. The second phase was quantitatively comparing the mapping. To do this, we compare the number of overlapping pixels between rasterized versions of each mappers' line work with different buffer widths. We find a range of 18 to 54% consistency between remote maps with 1m buffers. The percent overlap increases with buffer width and is higher in areas where the surface rupture was simpler with more vertical offset than areas with complex rupture patterns and/or little vertical offset. In general, field observations and aerial imagery detect more surface rupture features than airborne lidar. Lidar excels for detection and measurement of vertical offsets in the landscape, and it is deficient for detecting lateral offset with little or no vertical motion.

Intellectual Merit

Earthquake surface-rupture mapping provides essential data for seismic hazard evaluation and for understanding earthquake physics. Surface processes result in rapid smoothing and erasure of distributed deformation and fault scarps, requiring rapid field response to capture perishable data. As a result, few parts of a rupture are visited by more than one field team, leading to variable mapping detail and little to no information on the reproducibility of measured offsets. For the Ridgecrest Earthquake Sequence, we use post-earthquake lidar and imagery surveys to interpret and map the surface rupture. We compare results from multiple skilled mappers, and with independently collected field measurements, to objectively analyze the reproducibility of post-event maps.

Broader Impacts

This work will provide essential data for probabilistic fault displacement hazard assessments (PFDHA). This project provided summer research support and salary to UC Davis graduate students Alba M Rodriguez Padilla and Elaine K Young; was used as a teaching exercise and a graduate course on active tectonics during which course participants mapped a small part of

the rupture using only the lidar data; and facilitated and remote mapping experience to replace field course work for graduating senior Sergio Mendoza during Covid-19 shutdowns. Results from this project were presented at the 2020 and 2021 SCEC annual meetings and results and analysis contributed to three research publication (Rodriguez-Padilla et al., 2021, 2022, Young et al., in prep).

Technical Report

The primary goal of this project is to produce a map of the 2019 Ridgecrest sequence surface rupture generated by three independent mappers exclusively from lidar and other remotely sensed data. We use this map product to test the reproducibility of remote rupture maps and to compare with pre-event mapping and field-based mapping to further our understanding of mapped fault rupture locations. The large area covered by airborne lidar to document the 2019 Ridgecrest earthquake sequence (Figure 1; Hudnut et al., 2020) allows for detailed remote mapping covering regions far from the principal rupture trace. Understanding the quality and reproducibility of surface rupture maps covering these areas is important for guiding future field efforts in response to major earthquakes.

To begin, each of the three mappers set up a project in QGIS using the 2019 Ridgecrest lidar data. A variety of visualizations were used to view the topography (Figure 2). These visualizations included dynamically scaled elevation color ramps, slope shades, high-pass filtered elevations, and hillshade images with variable sun orientations and vertical exaggeration. We started with a 13 km section of the M7.1 rupture centered on the China Lake Naval base. Once all three mappers completely mapped the footprint of the lidar dataset, we compared the amount of overlap between each of the different maps (e.g., Figure 3).

To assess percent overlap in rupture maps we first created buffers around each of the mappers' line shapefiles. These buffers were 1m, 2m, 3m, 4m, 5m, 10m, and 15m. We then converted each of these buffered shapefiles into 0.5m-pixel rasters. This rasterization removes variability in line length and the buffers allows for subtle variations in line placement when mapping the same feature. Rasterization also removes the continuity of lines when mapping a single feature from the analysis, allowing us to focus exclusively on comparing whether a feature was mapped in that location. We calculate the amount of pixel overlap between a primary rasterized map and secondary rasterized map with buffer (Table 1). The number of shared pixels divided by the total number of pixels in the primary map yields the percent overlap. Our individual maps tend to agree with each other between 18% and 54% with 1m buffers. This increases to between 40% and 72% with 5m buffers. Percent overlap tends to plateau with increasing buffer widths above 5m. We also compared overlap for three sub-regions of the lidar dataset: the northern, central, and southern areas. The surface rupture is most discrete and has the highest vertical offset through the central region, which is reflected in higher percent overlap between maps for that area compared to the north or the south. The southern area has the least amount of overlap. Map disagreement depends largely on the number and location of ruptures mapped, rather than differences in mapping of the same features. In other words, location accuracy is good, but interpretation of what features constitute the rupture varies. When compared with rupture maps compiled using field data, the differences in location of lines mapped is often a function of what is visible in the field versus in the lidar. Field observations detect scarps that are shorter and accommodate less vertical offset

than can be discriminated from laser altimetry, as well as small fissures and secondary fractures without vertical offset. Such features would be missed by our mapping efforts. From parallel mapping efforts, we find that the number and extent of fault ruptures evident in drone- and aircraft collected- photography greatly exceeds that detectable from the lidar data.

Figures

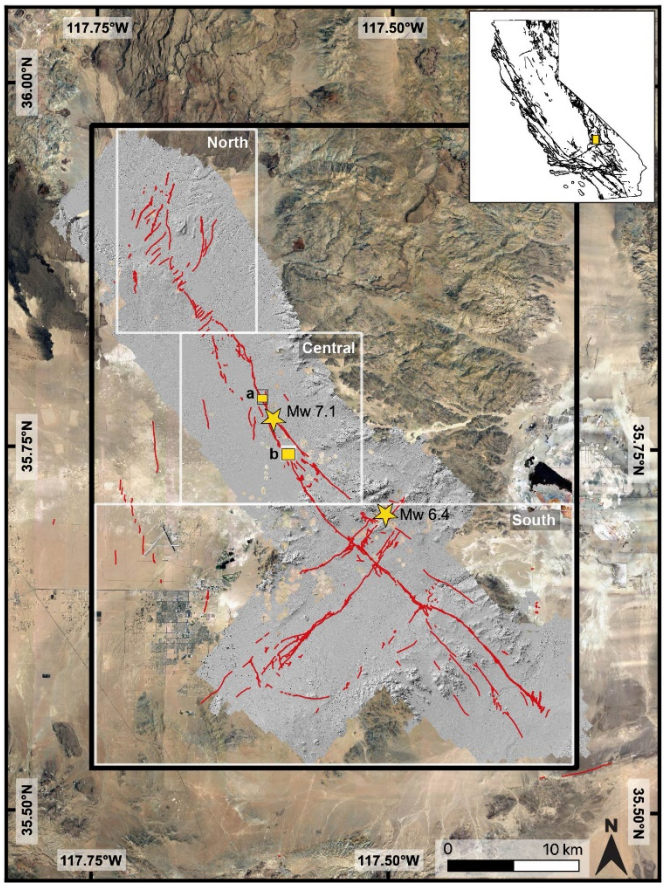

Figure 1. Map of Ridgecrest earthquake rupture. Greyscale hillshade image shows extent of post-event lidar (Hudnut et al., 2020). Red lines are the surface rupture map by Ponti et al. (2020). Yellow stars indicate the epicenter locations. The black box shows the entire extent of area analyzed. White boxes show the smaller areas analyzed: northern, central, and southern. Locations a and b are referenced in later figures. The white box at b is another area compared. Satellite imagery from Google Earth. Inset map shows Quaternary active faults of California. Solid yellow box indicates extent of larger map and location of Ridgecrest earthquakes in California.

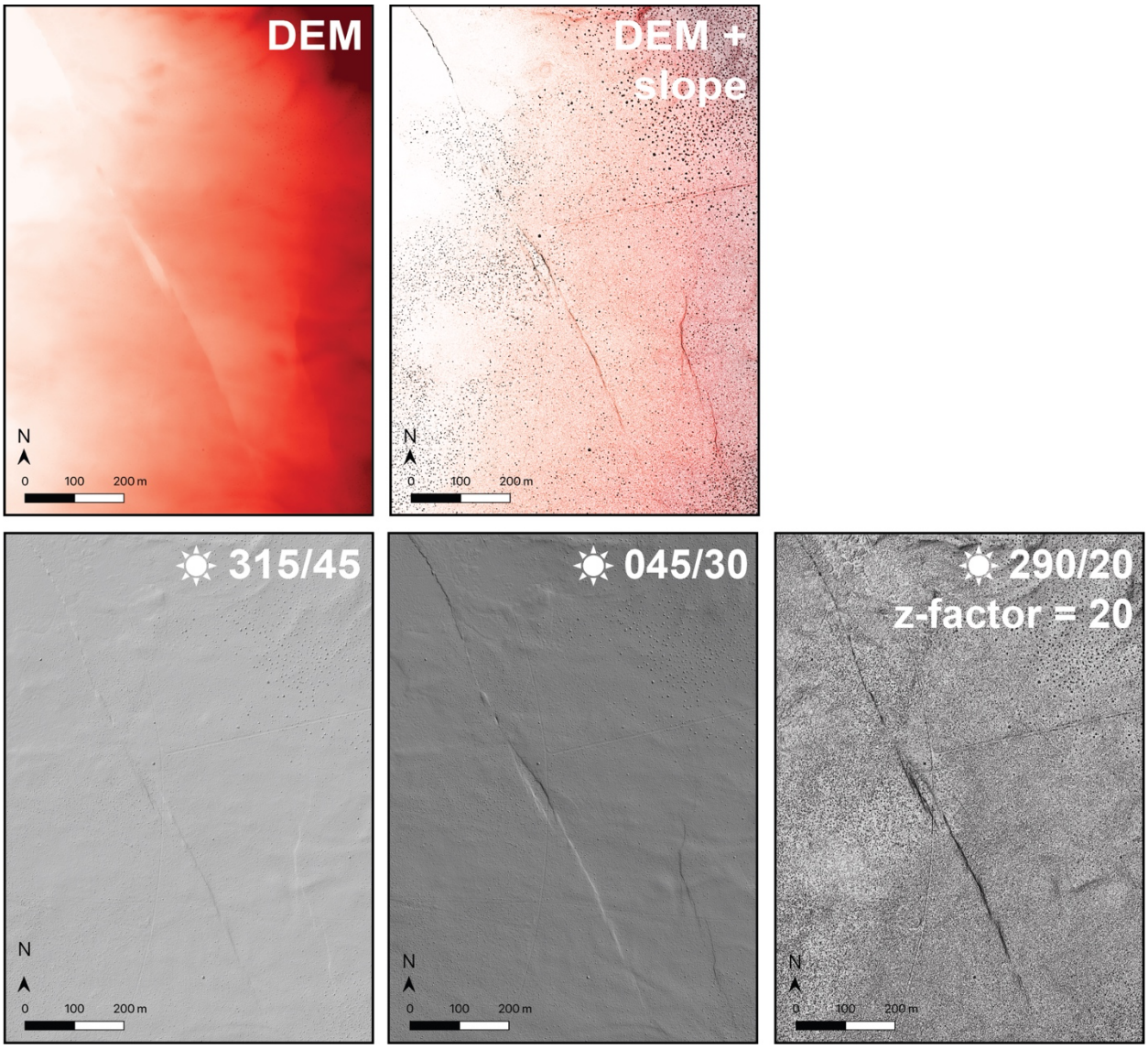

Figure 2. From top left to bottom right: DEM with dynamic red color ramp. Single-hued color ramp (red shown here) avoids bias of multi-hued color ramps. Dynamic color ramp adjusts to show full range of colors at every viewing scale. Digital Elevation Model (DEM) + transparent slopemap with values > 40% shown as black. Hillshade with default sun azimuth of 315° and altitude of 45°. Hillshade with adjusted sun azimuth of 045° and altitude of 30°. Hillshade with 20x vertical exaggeration and 20° sun altitude.

Figure 3. (next page) Two examples of mapping along the surface rupture. Locations a and b are shown in figure 1. Topographic show the importance of vertical displacement for mapping the surface rupture in the lidar. Gray triangles indicate position of intersections between the mapped surface rupture and the line of section. Line segments above the gray triangles use the same symbology as the map and indicate which mappers have lines at that location. Locations where all three remote mappers consistently mapped the surface rupture correspond to a steep fault scarp in the topographic profiles. The locations were only Ponti et al. (2020) maps the surface rupture are places where there is little vertical change in the topography.

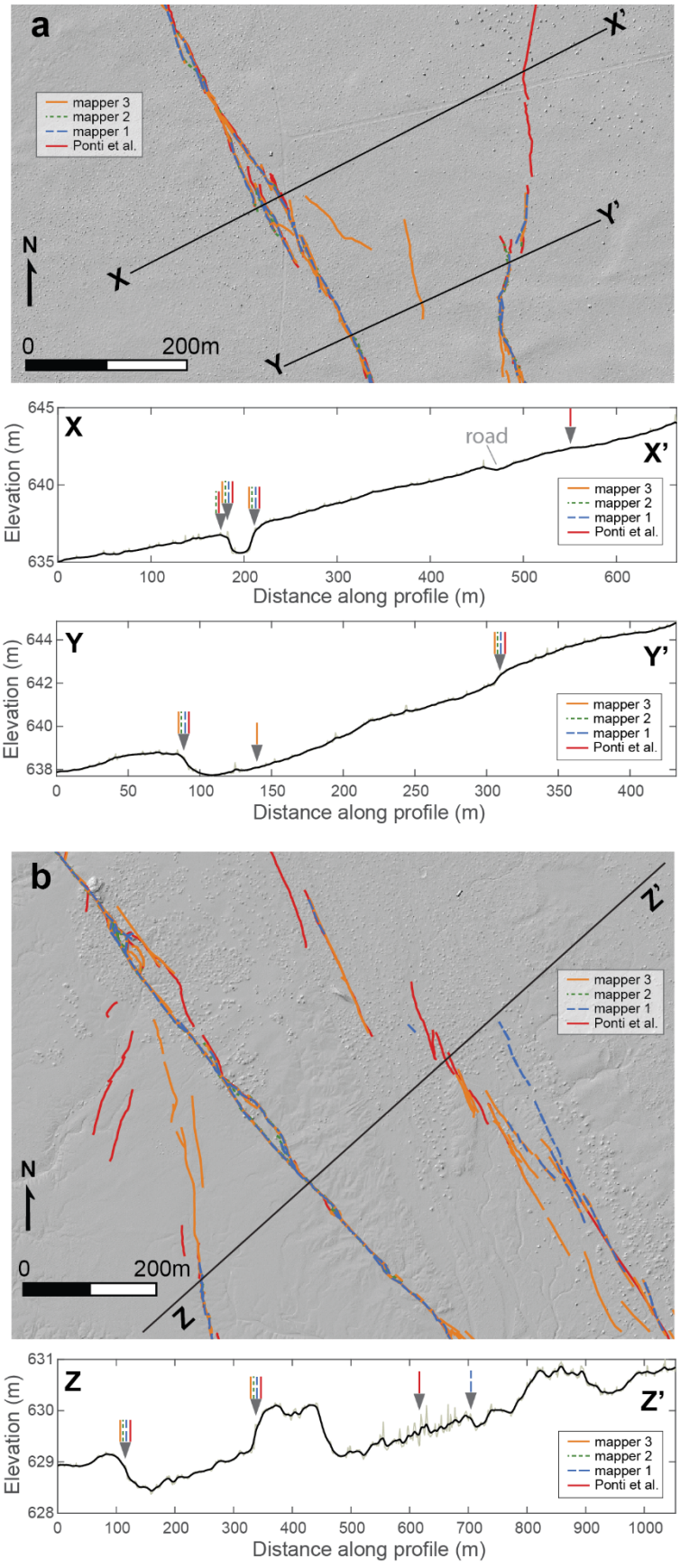
a
mapper 3
mapper 2
mapper 1
Ponti et al.
N
0
200m
X
X'
Y
Y'
Elevation (m)
road
Distance along profile (m)
b
Z
Z'

Area		Whole Map				North				Central				South				location b			
	pixels in lines	331048	271207	351694	816506	74756	40702	43728	128745	98289	123257	169985	164264	153771	107248	130727	504356	6315	8094	12701	10455
mapper	buffer width	M 1	M 2	M 3	P	M 1	M 2	M 3	P	M 1	M 2	M 3	P	M 1	M 2	M 3	P	M 1	M 2	M 3	P
M1	1m	-	36.8	30.9	8	-	23.8	23.5	3.7	-	47	35.6	17.7	-	30.1	28.9	6.2	-	76	43.8	38.5
	2m	-	47	39.3	12.3	-	31.7	32.1	6.2	-	57.8	43.8	25.9	-	40.4	38	9.9	-	89.6	52.5	47.5
	3m	-	51.9	44.1	15.5	-	36.1	37.9	8.3	-	62.8	48.5	31.4	-	45.3	42.7	12.7	-	93.3	56.4	51.4
	4m	-	55.1	47	18	-	39	40.9	9.9	-	66.2	51.4	35.6	-	48.4	45.7	15.1	-	94.9	58.3	54
	5m	-	57.5	49.2	20.2	-	41	43	11.4	-	68.6	53.8	39	-	50.9	47.9	17.1	-	96	60.3	55.2
	10m	-	64.4	55.8	27.4	-	48.1	48.7	19.2	-	75	60.3	47.8	-	58.4	55.3	23.9	-	97.7	64.5	59.5
	15m	-	68.4	60.1	31.6	-	51.6	51.6	22.5	-	78.7	65	52.4	-	62.8	59.8	28.3	-	98.5	68.8	63
M2	1m	27.4	-	39.7	8.2	12.7	-	27.9	3.6	50.8	-	44.9	21.2	20.3	-	39.1	5.4	66	-	44.9	44.9
	2m	32.1	-	45.7	11.7	16.2	-	33	5.3	56.2	-	50	27.6	25.2	-	47	8.4	67.8	-	46.6	47.6
	3m	33.7	-	48.4	14.2	17.9	-	35.3	6.7	58.2	-	52.7	32.5	26.7	-	50	10.6	69	-	48.4	49.5
	4m	34.7	-	50.1	16.1	18.9	-	36.7	8	59.2	-	54.4	35.7	27.6	-	51.9	12.3	69.8	-	49	50.1
	5m	35.4	-	51.5	17.6	19.5	-	37.7	9.3	59.9	-	55.6	38.3	28.4	-	53.6	13.7	69.9	-	49.4	50.7
	10m	37.5	-	55.2	22.7	21.2	-	40.3	14.2	62.3	-	59	44.3	30.5	-	58.3	18.7	70.2	-	50.8	51.9
	15m	37.5	-	55.2	22.7	21.2	-	40.3	14.2	62.3	-	59	44.3	30.5	-	58.3	18.7	70.2	-	50.8	51.9
M3	1m	31.6	53.9	-	9.5	13.6	30.3	-	3.3	58.4	67	-	24.6	24	47.8	-	6.5	80.4	90.3	-	59.2
	2m	38.2	63.4	-	14	18.3	36.2	-	4.9	67.3	76.5	-	34.4	30.2	58.6	-	10.2	87.7	96.5	-	66.8
	3m	41.1	67.5	-	17.3	21.1	39	-	6.2	71	80.6	-	40.9	32.8	63.3	-	13.1	88.7	98.3	-	70.1
	4m	42.6	70	-	19.9	22.7	41	-	7.5	72.8	83	-	45.6	33.9	66.1	-	15.4	89.2	98.9	-	71.6
	5m	43.5	71.8	-	21.9	23.7	42.3	-	8.7	74	84.7	-	49.1	34.7	68.2	-	17.2	90	99.5	-	73.2
	10m	46.6	75.9	-	27.9	26.6	45.5	-	13.6	77.2	88	-	56.6	37.8	73.6	-	23.2	92	100	-	76.1
	15m	48.5	78	-	30.7	28.1	47.2	-	15.2	79.4	89.6	-	60.3	39.8	76.3	-	26.2	93.1	100	-	77.8
P	1m	18.3	25.3	21.1	-	6.1	11	9.2	-	28.4	31.5	23.7	-	18.2	23.5	22.9	-	61.2	76.6	50.9	-
	2m	26.2	36.8	30.8	-	9.7	15.7	13.1	-	39.8	44.6	34.4	-	26.3	35.8	33.9	-	72.9	92.2	61.1	-
	3m	31.6	44.6	38.4	-	12.5	19.5	16.7	-	47.4	53.1	42.3	-	31.7	44.5	42.6	-	77.5	96.8	65.2	-
	4m	35.7	50.5	43.9	-	14.9	23.6	20.2	-	53.1	59.4	48	-	35.8	50.6	49	-	79.5	98.2	67.9	-
	5m	39.3	55.3	48.3	-	17	27.5	23.6	-	58	64.4	52.6	-	39.4	55.4	53.6	-	80.8	99.1	70.7	-
	10m	50.2	69.2	60.9	-	23.3	45.3	37.5	-	69.2	75.1	63.7	-	50.1	71.6	68.5	-	86.6	100	77.9	-
	15m	54.8	75.5	66.1	-	32.3	52.8	41.4	-	73.6	79.8	69	-	55.3	79.3	74.3	-	88.7	100	81	-

Table 1. Percent overlap between buffered (rows) and unbuffered (columns) rupture maps. We compared the entire map as well as smaller subregions (locales indicated along the top). Table cell colors vary depending on percent overlap (green = highest overlap; red = least overlap). The central part of the rupture where there is the most vertical displacement has the most agreement. Location B is a small, one-kilometer rupture section with an especially prominent scarp and highest levels of map agreement. The northern and southern areas, where deformation was more distributed and there is less vertical displacement, exhibit lower agreement. This is especially true when remote mapping is compared with the Ponti et al. 2020 map. M 1,2,3 = Mapper 1,2,3; P = Ponti et al., (2020)

References

Hudnut, K.W., B. Brooks, K. Scharer, J.L. Hernandez, T.E. Dawson, M.E. Oskin, R. Arrowsmith, C.A. Goulet, K. Blake, M.L. Boggs, S. Bork, C.L. Glennie, J.C. Fernandez-Diaz, A. Singhania, D. Hauser, S. Sorhus (2020). 2019 Ridgecrest, CA Post-Earthquake Lidar Collection. National Center for Airborne Laser Mapping (NCALM). Distributed by OpenTopography. https://doi.org/10.5069/G9W0942Z. Accessed: 2020-06-18

Ponti, D. J. et al., 2020, Documentation of Surface Fault Rupture and Ground-Deformation Features Produced by the 4 and 5 July 2019 Mw 6.4 and Mw 7.1 Ridgecrest Earthquake Sequence, Seismological Research Letters, 91, no. 5, 2942–2959, doi: 10.1785/0220190322.

Rodriguez Padilla, A. M., Oskin, M. E., Milliner, C. W. D. & Plesch, A. Accrual of widespread rock damage from the 2019 Ridgecrest earthquakes. Nat. Geosci. 15, 222–226 (2022).

Rodriguez Padilla, A. M. et al. Near-Field High-Resolution Maps of the Ridgecrest Earthquakes from Aerial Imagery. Seismological Research Letters 93, 494–499 (2021).